RSC Advances

PAPER

View Article Online
View Journal | View Issue

Cite this: *RSC Adv.*, 2018, **8**, 3530

Tunable emission from green to red in the $GdSr_2AlO_5:Tb^{3+},Eu^{3+}$ phosphor *via* efficient energy transfer

Yu Zhang, Xuejie Zhang, Haoran Zhang, Lingling Zheng, Yuan Zeng, Yu Lin, Yingliang Liu * and Bingfu Lei *

Received 9th November 2017
Accepted 26th December 2017

DOI: 10.1039/c7ra12260h

rsc.li/rsc-advances

Herein, a series of $GdSr_2AlO_5:Tb^{3+},Eu^{3+}$ phosphors were successfully synthesized through a high temperature solid-state reaction, and their crystal structures as well as photoluminescence properties were investigated in detail. Compared to the intense emission of $^5D_0 \rightarrow {}^7F_1$ or $^5D_0 \rightarrow {}^7F_2$ transition of Eu^{3+}, another strong emission corresponding to $^5D_0 \rightarrow {}^7F_4$ was observed. Concentration quenching is not obvious in Tb^{3+} or Eu^{3+}-doped $GdSr_2AlO_5$ because structure isolation and energy transfer (ET) of $Gd^{3+} \rightarrow Eu^{3+}$ and $Gd^{3+} \rightarrow Tb^{3+}$ were found. Moreover, the energy transfer process from Tb^{3+} to Eu^{3+} was verified by the overlap of luminescence spectra and the variation of lifetime. Energy transfer mechanism was determined to be a dipole–dipole interaction, and ET efficiency as well as quantum efficiency were also obtained. Moreover, the emission color of $GdSr_2AlO_5:Tb^{3+},Eu^{3+}$ can be tuned from green to red by altering the ratio of Tb^{3+}/Eu^{3+}. These results indicate that the $GdSr_2AlO_5:Tb^{3+},Eu^{3+}$ phosphor is a promising single-component white light-emitting phosphor.

1. Introduction

White light-emitting diodes (w-LEDs) with superior advantages, such as high energy efficiency, good physical and chemical stability, long lifetime, and environment friendliness, have been drawing attention and are regarded as the next generation of illumination sources.[1–4] The most available material for light devices involves Ce^{3+}-doped yttrium aluminum garnet ($YAG:Ce^{3+}$) with blue-LED chips, which has been commercialized.[5,6] Because of the scarcity of red component, it encounters a low color rendering index ($R_a < 80$) and a high color temperature (CCT > 7000 K).[7,8] To overcome these drawbacks, the combination of a UV LED chip with red ($Ca_4(PO_4)O:Eu^{2+}$),[9] green ($Na_2Y_2B_2O_7:Ce^{3+},Tb^{3+}$),[10] and blue ($Na_xCa_{1-x}Al_{2-x}Si_{2+x}O_8:Eu^{2+}$)[11] to achieve white-light with high R_a and appropriate CCT is another approach. However, the mixture of different phosphors brings about an inevitable problem of fluorescence reabsorption, resulting in the loss of luminous efficiency.[12,13] Therefore, it is obligatory to develop a single-phase white light-emitting phosphor.

Rare earth ion-doped aluminate phosphors, such as $LaSr_2AlO_5:Ce^{3+}/Eu^{2+}$,[14,15] $(La,Gd)Sr_2AlO_5:Ce$,[16] and $(La,Gd)Sr_2(Al,B)O_5:Ce$,[17] have been studied extensively due to their cheap raw materials and good chemical and physical stability. The structural properties of this aluminate-based phosphor and the effect on the luminescence properties have been investigated. However, the luminescence of Ce^{3+} and Eu^{2+} belong to the f–d transition.[18] Upon reviewing the literature, it is observed that it is difficult to find other rare-earth ions with f–f transition for doping into the $GdSr_2AlO_5$ phosphor. As is well known, co-doping of different rare ions as a sensitizer and activator plays a significant role in obtaining emission *via* energy transfer processes.[19]

Tb^{3+} and Eu^{3+} with characteristic green[20,21] and red[22,23] emissions are widely used in luminescent materials, respectively. Compared to most Eu^{3+}-doped phosphors with the dominant emission corresponding to $^5D_0 \rightarrow {}^7F_1$ or $^5D_0 \rightarrow {}^7F_2$, the Eu^{3+}-doped $GdSr_2AlO_5$ phosphor shows an intensive emission related to $^5D_0 \rightarrow {}^7F_4$. It is clear that Tb^{3+} functions as a good sensitizer to improve the luminescence efficiency of Eu^{3+} ions in $Sr_2MgSi_2O_7$,[24] $Na_3La(PO_4)_2$,[25] $CaYAlO_4$,[26] and Y_2O_3 (ref. 27) phosphors. In this study, a single-phased $GdSr_2AlO_5:Tb^{3+},Eu^{3+}$ phosphor was synthesized by a conventional solid-state method. The efficient energy transfer from Tb^{3+} to Eu^{3+} was systematically investigated with steady state fluorescence, lifetime measurement, and the energy transfer efficiency. Moreover, the color of the total emission can be tuned by altering the ratio of Tb^{3+}/Eu^{3+} in the $GdSr_2AlO_5$ host.

2. Experimental method

A series of phosphors with the composition of $GdSr_2AlO_5:Tb^{3+}$, $GdSr_2AlO_5:Eu^{3+}$, and $GdSr_2AlO_5:Tb^{3+},Eu^{3+}$ were prepared by a conventional high temperature solid-state method under

Guangdong Provincial Engineering Technology Research Center for Optical Agricultural, College of Materials and Energy, South China Agriculture University, Guangzhou 510642, P. R. China. E-mail: tleibf@scau.edu.cn

a reductive atmosphere (5% H_2 + 95% N_2) at 1500 °C. $SrCO_3$ (A. R.), Al_2O_3 (A. R.), Gd_2O_3 (A. R.), Tb_4O_7 (99.99%), and Eu_2O_3 (99.99%) were used as raw materials. They were stoichiometrically weighed and mixed by grinding in an agate mortar for 30 min. After this, they were transferred into ceramic crucibles and calcined in a high-temperature tubular furnace at 1500 °C for 4 h at a heating rate of 3 °C min^{-1}. Finally, the samples were cooled down to room temperature in the furnace and ground into powders for subsequent use.

Bruker D8 (voltage 40 kV and current 40 mA) over the 2θ range from 10° to 70° with CuKα radiation ($\lambda = 1.54178$ Å) was used to obtain the XRD patterns of $GdSr_2AlO_5$:Tb^{3+},Eu^{3+} samples. Hitachi F-7000 spectrophotometers with a 150 W xenon lamp light source were used to obtain the excitation and emission spectra. The morphology of the prepared phosphor was examined by a field-emission scanning electron microscope (Hitachi S-4800). The decay curves were obtained using the Hamamatsu Quantaurus-Tau C11367 fluorescence spectrophotometer. The chromaticity data were calculated by the CIE1931 software. Photoluminescence absolute quantum efficiency (QE) was determined *via* Hamamatsu Quantaurus-QY C11347 using an integrated sphere. All the measurements were conducted at room temperature.

3. Results and discussion

3.1 XRD analysis

Fig. 1(a) shows the XRD patterns of the as-prepared $GdSr_2AlO_5$ host and Tb^{3+}, Eu^{3+}-doped phosphor as well as the standard patterns of $EuSr_2AlO_5$ (JCPDS 70-2197). The patterns agreed with the crystallographic structure of the JCPDS card 70-2197, and impurity peaks were not found. This result illustrates that the obtained samples are in single phase, and doping of Tb^{3+} and/or Eu^{3+} ions at low concentrations does not change the crystal structure. In addition, it can be observed from Fig. 1(b) that the diffraction peak positions of the samples are shifted slightly to a higher angle as compared to those of the standard patterns of $EuSr_2AlO_5$ (JCPDS 70-2197); this can be due to the replacement of large-size Eu^{3+} sites by the smaller-size trivalent ions. Hence, RE^{3+} ions were effectively doped into the lattice; this could be confirmed by the slight change in the diffraction peaks.

Fig. 1(c) displays a partial structure of $GdSr_2AlO_5$. As reported previously, the crystal structure of $GdSr_2AlO_5$ is isostructural with the standard file of $EuSr_2AlO_5$ (JCPDS no. 70-2197, tetragonal, space group *I*4/*mcm*).[28] Gd atoms will occupy the half 8h sites, and the other half is occupied by the Sr atoms. The cell also contains 4a sites, which are fully occupied by the Sr atoms, and the Al atoms will occupy the 4b sites. The 4c sites and 16l sites are occupied by O, denoted as O_1 and O_2, respectively. The GdO_8 polyhedron consists of two O_1 atoms and six O_2 atoms, where the latter are shared by four AlO_4 tetrahedral on the adjacent layers, forming an isolated structure. Fortunately, isolation in space weakens the interaction between the paired ions. To some extent, the concentrating quenching effect would be avoided.[29]

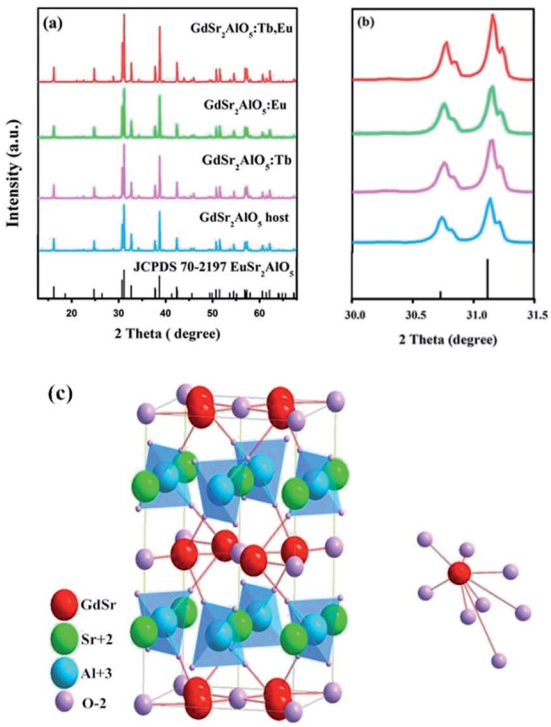

Fig. 1 (a) Representative XRD patterns of the samples. (b) Magnified XRD patterns between 30° and 31.5°. (c) Crystal structure of the $GdSr_2AlO_5$ and the coordination environment of GdO_8.

3.2 SEM with energy dispersive X-ray analysis

Fig. 2(a) displays the morphology of the $GdSr_2AlO_5$:Tb^{3+},Eu^{3+} sample. The surface image shows irregular particles with a size range of 5–10 μm. Moreover, as shown in Fig. 2(b), EDS is used to analyze the chemical composition of the $GdSr_2AlO_5$:Tb^{3+},Eu^{3+} phosphor, and the result confirms the presence of Gd, Sr, Al, O, Tb, and Eu elements in the phosphor. Compared with the abovementioned XRD results, the EDS results demonstrate that Tb/Eu ions have been successfully incorporated into the $GdSr_2AlO_5$ lattice.

3.3 Luminescence properties

The excitation spectrum of $GdSr_2AlO_5$:2%Tb^{3+} is shown in Fig. 3(a). The excitation spectrum monitored at 548 nm exhibits a broad band and several weak peaks. The broad band from

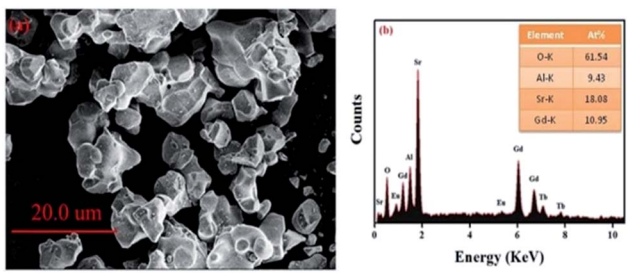

Fig. 2 SEM image (a) and EDS spectrum (b) of $GdSr_2AlO_5$:2%Tb^{3+},2% Eu^{3+}.

200 nm to 250 nm centered at 220 nm is ascribed to the f–d transitions of the Tb^{3+} ions, whereas the excitation peaks at 275 and 310 nm originate from the transitions of $^8S_{7/2} \rightarrow {}^6I_{7/2}$ and $^8S_{7/2} \rightarrow {}^6P_{7/2}$ of the Gd^{3+} ions, respectively.[30,31] The appearance of strong excitation sharp bands of Gd^{3+} ions confirms that there is an efficient energy transfer from Gd^{3+} to Tb^{3+}. The emission spectra of the phosphor under 220, 275, and 310 nm excitation in the wavelength range from 400–650 nm are also depicted in Fig. 3(a). There are two groups of lines in the emission spectrum: one group in the region from 400 to 480 nm is derived from the $^5D_3 \rightarrow {}^7F_J$ ($J = 5$, 4, and 3) transitions of Tb^{3+}. The second groups of lines in the wavelength range from 480 to 650 nm originate from the $^5D_4 \rightarrow {}^7F_J$ ($J = 6$, 5, 4, and 3) transitions. Among these emissions, the $^5D_4 \rightarrow {}^7F_5$ transition with a maximum at about 548 nm exhibits the strongest emission intensity. The emission intensity increases with the increasing concentration of Tb^{3+}, as presented in Fig. 3(b). Concentration quenching does not occur in $GdSr_2AlO_5$:Tb^{3+}.

Fig. 3(c) and (d) present the excitation and emission spectra as well as concentration-dependent luminescence intensity of $GdSr_2AlO_5$:yEu^{3+}. The excitation spectrum of the Eu^{3+}-activated sample monitoring the emission wavelength at 705 nm contains a broad band in the wavelength range from 220 to 350 nm, corresponding to the charge transfer transition of Eu^{3+} ($O^{2-} \rightarrow Eu^{3+}$) and several characteristic narrow peaks at 383 nm and 393 nm. They are attributed to $^7F_0 \rightarrow {}^5G_2$ and $^7F_0 \rightarrow {}^5L_6$ electronic transitions of the Eu^{3+} ions. In this band, there should be absorption of transitions from $^8S_{7/2}$ to $^6I_{7/2}$ level of Gd^{3+}, which is too weak and is overlapped with the strong CTB of the $O^{2-} \rightarrow Eu^{3+}$.[32,33] The emission spectrum consists of multiple band emissions at 587, 607, 622, 657, and 705 nm, which are assigned to the $^5D_0 \rightarrow {}^7F_J$ ($J = 0$, 1, 2, 3, and 4) transitions of Eu^{3+} ions,[34] respectively. Among these emission peaks, the two most intense lines are the emissions located at 622 and 705 nm. Obviously, the magnetic dipole transition of $^5D_0 \rightarrow {}^7F_1$ is stronger than the $^5D_0 \rightarrow {}^7F_2$ electronic transition; this indicates that Eu^{3+} ions in the $GdSr_2AlO_5$ host occupy a site with a non-inversion symmetry; this is consistent with its structure. Compared to other Eu^{3+} phosphors, $GdSr_2AlO_5$:Eu^{3+} provides more red components to improve R_a. Similarly, there is no evident concentration quenching with the change in the Eu^{3+} concentration.

The foundation of energy transfer is the spectral overlapping Tb^{3+} emission and the Eu^{3+} excitation. As is clearly shown in Fig. 4, there are some overlaps between the emission of $^5D_3 \rightarrow {}^7F_6$ (Tb^{3+}) and the excitation of $^7F_0 \rightarrow {}^5G_{2,3,4,5}$, $^5L_8$ (Eu^{3+}). Moreover, the excitation of $^7F_0 \rightarrow {}^5D_3$, $^5L_6$ (Eu^{3+}) overlaps with the emission of $^5D_3 \rightarrow {}^7F_5$ (Tb^{3+}).[35]

To further investigate the energy transfer process, a series of samples of $GdSr_2AlO_5$:2%Tb^{3+},x%Eu^{3+} ($x = 0$, 0.5, 1, 2, 3, and 5) were prepared whose emission spectra under the excitation at 275 nm are presented in Fig. 5(a). The characteristic sharp emission peaks of Tb^{3+} and Eu^{3+} are observed. The tendency in the variation of Tb^{3+} and Eu^{3+} differs significantly. The emission intensity of Tb^{3+} at 548 nm decreases remarkably with an increase in the concentration of Eu^{3+}, whereas the emission intensity of Eu^{3+} increases monotonously. Fig. 5(b) depicts the contribution of different ions in the corresponding emission spectra. The G/R (green to red) ratio continuously decreases notably. Based on the prerequisite of the concentration of Tb^{3+} being a constant value, explanation for this phenomenon should be the evidence of energy transfer from Tb^{3+} to Eu^{3+}.

In spite of steady-state spectra, kinetic spectra are necessary to better analyze the energy transfer mechanism of $Tb^{3+} \rightarrow Eu^{3+}$ in $GdSr_2AlO_5$. Fig. 6(a) shows the fluorescence decay curves of Tb^{3+} emissions, which are obtained under 275 nm excitation and detected at 548 nm. The luminescence curves can be fitted well with the double-exponential expression:[36,37]

$$I(t) = I_0 + A_1 \exp(-t/\tau_1) + A_2 \exp(-t/\tau_2) \quad (1)$$

where I and I_0 represent the luminescence intensity at time t and 0, A_1 and A_2 are equal to constants, t is the time, and τ_1 and τ_2 are the rapid and slow lifetimes for exponential components, respectively. As a function of these parameters, the average luminescence lifetime (τ) was determined by the following equation:

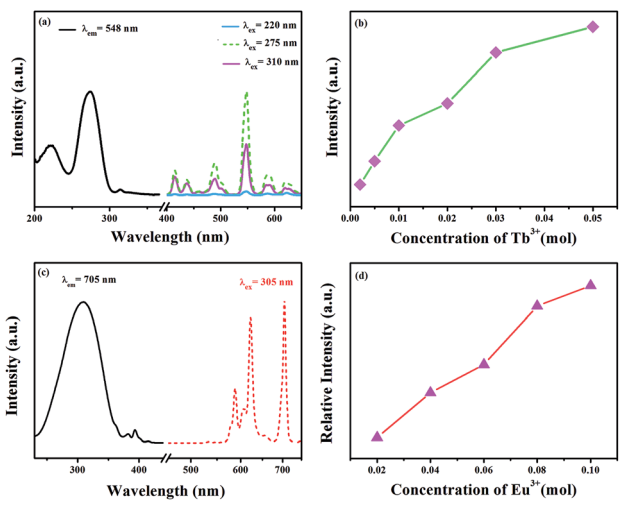

Fig. 3 (a) Excitation and emission spectra of the $GdSr_2AlO_5$:2%Tb^{3+} phosphor. (b) Concentration-dependent luminescence intensity of $GdSr_2AlO_5$:xTb^{3+}. (c) Excitation and emission spectra of the $GdSr_2AlO_5$:2%Eu^{3+} phosphor and (d) concentration-dependent luminescence intensity of $GdSr_2AlO_5$:yEu^{3+}.

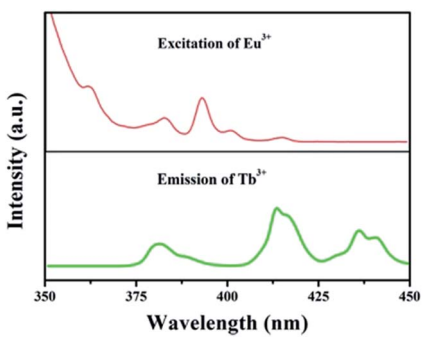

Fig. 4 Spectral overlapping of the PL spectrum of $GdSr_2AlO_5$:Tb^{3+} and the PLE spectrum of $GdSr_2AlO_5$:Eu^{3+}.

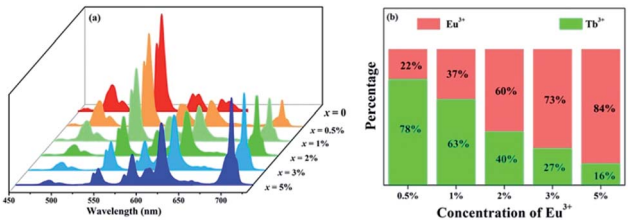

Fig. 5 (a) Emission spectra of $GdSr_2AlO_5$:2%Tb^{3+},x%Eu^{3+} ($x = 0$, 0.5, 1, 2, 3, and 5) under 275 nm excitation. (b) Variation tendency of the green emission of Tb^{3+} and the red emission of Eu^{3+}.

$$\tau = (A_1\tau_1^2 + A_2\tau_2^2)/(A_1\tau_1 + A_2\tau_2) \quad (2)$$

The values of τ are calculated to decrease when the Eu^{3+} concentration increases; this indicates that energy transfer occurs from Tb^{3+} to Eu^{3+}, as expected. Furthermore, the energy transfer efficiency is calculated by the expression as follows:[38]

$$\eta_T = 1 - I_s/I_{so} \quad (3)$$

where η_T represents the energy transfer efficiency, and I_s and I_{so} represent the luminescence intensity of Tb^{3+} in the presence and absence of Eu^{3+}, respectively. The results of η_T are shown in Fig. 6(b). It can be found that the efficiencies from Tb^{3+} to Eu^{3+} increase with the increasing Eu^{3+} concentration, which can reach the maximum value of 83%. Therefore, the energy transfer from Tb^{3+} to Eu^{3+} ions is efficient to improve Eu^{3+} luminescence.

3.4 Energy transfer mechanism

The type of energy transfer should depend on either the exchange interaction or the multipolar interaction. It relies on the critical distance between the Tb^{3+} (sensitizer) and Eu^{3+} (activator), and the critical distance is expressed by the following formula:[39]

$$R_{Tb-Eu} = 2\left[\frac{3V}{4\pi x_c N}\right]^{1/3} \quad (4)$$

where V represents the cell volume, N is equal to the number of cations in the unit cell, and x_c is the total concentration of Tb^{3+} and Eu^{3+}. In this case, $N = 4$ and $V = 498.64$ Å^3. The corresponding distance is calculated to be more than 5 Å, indicating that $Tb^{3+} \rightarrow Eu^{3+}$ energy transfer would tend to be a multipolar interaction. On account of energy transfer mechanism for multipolar interaction, the following expression can be given:[40,41]

$$I_{so}/I_s \propto C^{n/3} \quad (5)$$

where I_{so} and I_s are the luminescence intensity of the sensitizer without and with activator. C represents the doping concentration of Tb^{3+} and Eu^{3+} ion. The values for $n = 6$, 8, and 10 correspond to dipole–dipole, dipole–quadrupole, and quadrupole–quadrupole interactions. Results are illustrated in Fig. 7. The best linear fit was obtained when $n = 6$, which confirmed energy transfer through dipole–dipole mechanism.

The detailed $Gd^{3+} \rightarrow Tb^{3+}$, $Gd^{3+} \rightarrow Eu^{3+}$, and $Tb^{3+} \rightarrow Eu^{3+}$ energy transfer processes are shown in Fig. 8. The electrons were excited from the $^8S_{7/2}$ ground state to the ^6I_J excited state of Gd^{3+} under 275 nm excitation. Because the energy levels $^5D_3$ of Tb^{3+} and $^5D_1$ state of Eu^{3+} are lower than the ^6I_J state of Gd^{3+} in the diagram, the energy transfer processes from $Gd^{3+} \rightarrow Tb^{3+}$ and $Gd^{3+} \rightarrow Eu^{3+}$ occur simultaneously. In addition, the electrons absorbing energy were excited from the $^7F_6$ ground state to the $^5D_3$ excited state of Tb^{3+}. The energy transfer process occurs between Tb^{3+} and Eu^{3+} activators since the $^5D_3$ state of Tb^{3+} lies higher than the $^5D_1$ state of Eu^{3+}. Then, the electrons from the excited state of $^5D_3$ (Tb^{3+}) and $^5D_1$ (Eu^{3+}) relaxed to $^5D_4$ and $^5D_0$, respectively. Finally, green to red emission is yielded by electrons returning to their respective ground states.

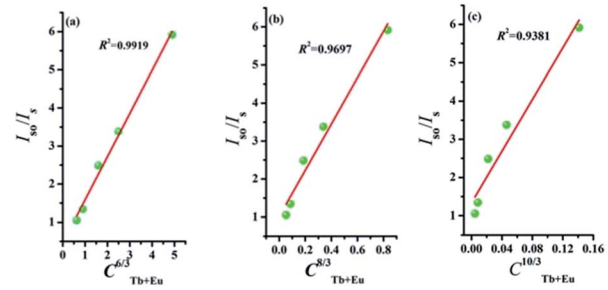

Fig. 7 Dependence of I_{so}/I_s of Tb^{3+} on (a) $C^{6/3}$, (b) $C^{8/3}$, and (c) $C^{10/3}$.

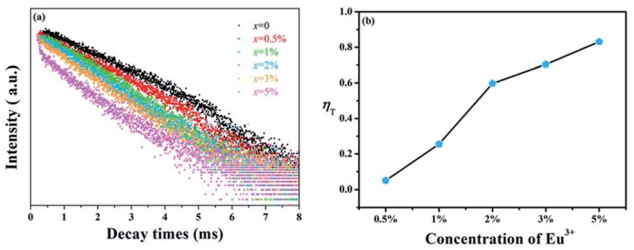

Fig. 6 (a) Decay curves of Tb^{3+} in $GdSr_2AlO_5$:2%Tb^{3+},x%Eu^{3+} ($x = 0$, 0.5, 1, 2, 3, and 5). (b) Energy transfer efficiencies (η_T) in $GdSr_2AlO_5$:2% Tb^{3+},x%Eu^{3+} as a function of different Eu^{3+} concentrations.

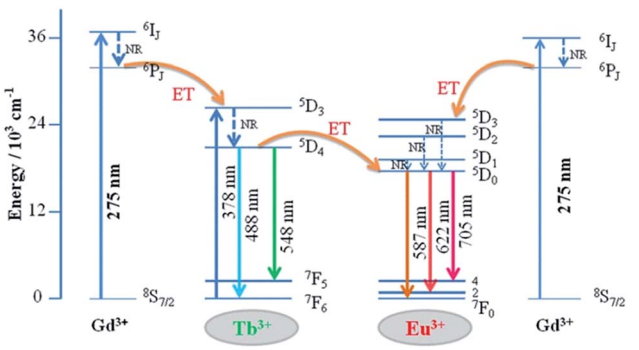

Fig. 8 Schematic of energy transfer from Tb^{3+} to Eu^{3+} in $GdSr_2AlO_5$.

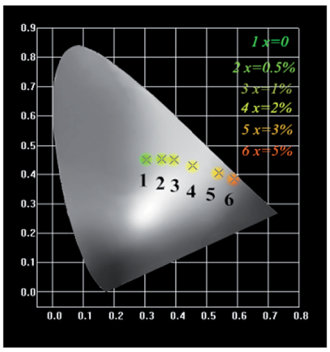

Fig. 9 CIE chromaticity diagram for $GdSr_2AlO_5$:2%Tb^{3+},x%Eu^{3+} ($x = 0$, 0.5, 1, 2, 3, and 5) samples.

3.5 CIE chromaticity coordinate and QE

The Commission Internationale de L'Eclairage (CIE 1931) chromaticity coordinates of $GdSr_2AlO_5$:2%Tb^{3+},x%Eu^{3+} phosphors under the excitation at 275 nm are presented in Fig. 9. The CIE coordinates shifted from (0.320, 0.466) to (0.574, 0.403) for the samples $x = 0$ to $x = 5\%$ correspond to green, yellow-green, and red. It is clear that the coordinate Y changes linearly with the X, the expression of which can be shown as below:

$$Y = 0.7541 - 0.6109X \quad (6)$$

The equation proves that the range of chromaticity coordinates can be obtained by adjusting the ratio of Tb^{3+} and Eu^{3+} mathematically. The as-prepared phosphor emits bright tunable visible light, implying its potential application in multicolor displays, and meets the requirement for application in *n*-UV LEDs.

For photo-luminescence application, the importance of quantum efficiency (QE) should be considered. According to the method described by De Mello *et al.*, QE can be calculated by the following equation:[42]

$$\eta_{QE} = \frac{\int L_S}{\int E_R - \int E_S} \quad (7)$$

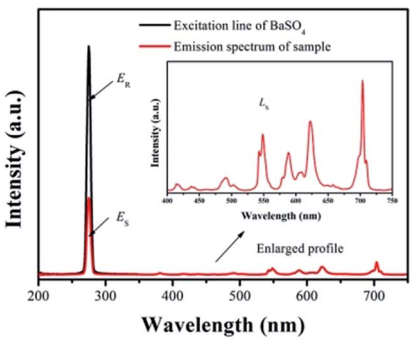

Fig. 10 Excitation line of $BaSO_4$ and emission spectrum of the sample. Inset shows the magnification of the emission spectrum.

where L_S is the emission of the sample, E_S equals to the spectrum of the sample excited by the light, and E_R represents the spectrum of the excitation light without the sample. The results are listed in Fig. 10. Under 275 nm sexcitation, the calculated QE of $GdSr_2AlO_5$:2%Tb^{3+},2%Eu^{3+} is 78.5%, which demonstrates a high QE.

4. Conclusions

The $GdSr_2AlO_5$:Tb^{3+},Eu^{3+} phosphors were prepared by a high temperature solid-state reaction method, and their luminescence properties were investigated in detail. Due to REO_8 structure isolation, damping of the concentration quenching would occur. Energy transfer from $Gd^{3+} \rightarrow Eu^{3+}$ and $Gd^{3+} \rightarrow Tb^{3+}$ was found in the excitation spectrum. Moreover, the luminescence properties and the transient spectra confirmed the efficiency energy transfer from Tb^{3+} to Eu^{3+}. The mechanism it demonstrated is dipole–dipole interaction. $GdSr_2AlO_5$:Tb^{3+},Eu^{3+} phosphors were able to provide multi-color emission from green, yellow, orange, and finally to deep red by the different ratios of Tb^{3+}/Eu^{3+}. Additionally, the QE can reach about 78.5%. All the results indicate that the series of $GdSr_2AlO_5$:Tb^{3+},Eu^{3+} phosphors can be a candidate for color tunable luminescence materials used for *n*-UV LEDs.

Conflicts of interest

There are no conflicts to declare.

Acknowledgements

The present work was supported by the National Natural Science Foundation of China (Grant No. 21671070, and 21571067), the Project for Construction of High-level University in Guangdong Province, the Teamwork Projects funded by the Guangdong Natural Science Foundation (Grant No. S2013030012842), the Guangzhou Science & Technology Project (No. 201704030086, 201605030005), and the Spectral Funds for the Cultivation of Guangdong College Student Scientific and Technological Innovation ("Climbing Program" Special Funds No. pdjh2017a0075).

References

1 W. Li, J. Wang, H. Zhang, Y. Liu, B. Lei, J. Zhuang, J. Cui, M. Peng and Y. Zhu, *RSC Adv.*, 2016, **6**, 33076–33082.
2 N. C. George, K. A. Denault and R. Seshadri, *Annu. Rev. Mater. Res.*, 2013, **43**, 481–501.
3 C. C. Lin and R. S. Liu, *J. Phys. Chem. Lett.*, 2011, **2**, 1268–1277.
4 M. Shang, C. Li and J. Lin, *Chem. Soc. Rev.*, 2014, **43**, 1372–1386.
5 A. A. Setlur, *Electrochem. Soc. Interface*, 2009, **18**, 32–36.
6 D. J. Robbins, *J. Electrochem. Soc.*, 1979, **126**, 1550–1555.
7 S. Nakamura, *MRS Bull.*, 2009, **34**, 101–107.
8 S. Nakamura, *Proc. SPIE*, 1997, **3002**, 26–35.

9 D. Deng, H. Yu, Y. Lin, Y. Hua, G. Jia and S. Zhao, *J. Mater. Chem. C*, 2013, **1**, 3194–3199.
10 D. Wen, H. Yang, G. Yang, J. Shi, M. Wu and Q. Su, *J. Solid State Chem.*, 2014, **213**, 65–71.
11 G. Lee, J. Y. Han, W. B. Im, S. H. Cheong and D. Y. Jeon, *Inorg. Chem.*, 2012, **51**, 10688–10694.
12 T. Nishida, T. Ban and N. Kobayashi, *Appl. Phys. Lett.*, 2003, **82**, 3817–3819.
13 Y. Liu, X. Zhang, Z. Hao, X. Wang and J. Zhang, *Chem. Commun.*, 2011, **47**, 10677–10679.
14 W. B. Im, N. N. Fellows, S. P. DenBaars, R. Seshadri and Y. Kim, *Chem. Mater.*, 2009, **21**, 2957–2966.
15 C. R. García, J. Oliva and L. A. Díaz-Torres, *Photochem. Photobiol.*, 2015, **91**, 505–509.
16 Z. Xia and Z. Yu, *J. Mater. Chem. C*, 2015, **44**, 11629–11634.
17 J. Hyun Kim and K. Youl Jung, *J. Lumin.*, 2012, **132**, 1376–1381.
18 G. Li, Y. Tian, Y. Zhao and J. Lin, *Chem. Soc. Rev.*, 2015, **44**, 8688–8713.
19 K. Li, M. Shang, H. Lian and J. Lin, *J. Mater. Chem. C*, 2016, **4**, 5507–5530.
20 X. Yang, B. Zhang, T. Xu, L. Wang, J. Shen and Q. Zhang, *J. Mater. Sci.: Mater. Electron.*, 2016, **27**, 9448–9453.
21 C. Zhang, H. Liang, S. Zhang, C. Liu, D. Hou, L. Zhou, G. Zhang and J. Shi, *J. Phys. Chem. C*, 2012, **116**, 15932–15937.
22 Y. Meng, W. Zhao, L. Wang, Y. Zhou, M. He and Y. Zhu, *J. Mater. Sci.: Mater. Electron.*, 2017, **28**, 4984–4989.
23 X. Zhou and X. Wang, *J. Lumin.*, 2014, **29**, 143–146.
24 K. Pavani, J. Suresh Kumar and L. Rama Moorthy, *J. Alloys Compd.*, 2014, **586**, 722–729.
25 D. Wang, Y. Wang and J. He, *Mater. Res. Bull.*, 2012, **47**, 142–145.
26 D. Geng, G. Li, M. Shang, C. Peng, Y. Zhang, Z. Cheng and J. Lin, *Dalton Trans.*, 2012, **41**, 378–386.
27 M. Back, M. Boffelli, A. Massari, R. Marin, F. Enrichi and P. Riello, *J. Nanopart. Res.*, 2013, **15**, 1753–1767.
28 L. S. D. Glasser and F. P. Glasser, *Acta Crystallogr.*, 1965, **18**, 453–455.
29 D. Wen, J. Feng, J. Li, J. Shi, M. Wu and Q. Su, *J. Mater. Chem. C*, 2015, **3**, 2107–2114.
30 H. Guan, G. Liu, J. Wang, X. Dong and W. Yu, *Dalton Trans.*, 2014, **43**, 181–188.
31 M. M. Yawalkar, G. D. Zade, V. Singh and S. J. Dhoble, *J. Mater. Sci.: Mater. Electron.*, 2017, **28**, 180–189.
32 J. Singh and J. Manam, *J. Mater. Sci.*, 2016, **51**, 2886–2901.
33 X. X. Li, Y. H. Wang and Z. Chen, *J. Alloys Compd.*, 2008, **453**, 392–394.
34 G. K. Behrh, R. Gautier, C. Latouche, S. Jobic and H. Serier-Brault, *Inorg. Chem.*, 2016, **55**, 9144–9146.
35 J. Li, Z. Zhang, X. Li, Y. Xu, Y. Ai, J. Shi and M. Wu, *J. Mater. Chem. C*, 2017, **5**, 6294–6299.
36 M. Yu, J. Lin and J. Fang, *Chem. Mater.*, 2005, **17**, 1783–1791.
37 X. Liu, C. Li, Z. Quan, Z. Cheng and J. Lin, *J. Phys. Chem. C*, 2007, **111**, 16601–16607.
38 M. Xu, L. Wang, D. Jia and H. Zhao, *J. Am. Ceram. Soc.*, 2015, **98**, 1536–1541.
39 S. P. Lee, C. H. Huang and T. Chen, *J. Phys. Chem. C*, 2014, **2**, 8925–8931.
40 D. L. Dexter and J. H. Schulman, *J. Chem. Phys.*, 1954, **22**, 1063–1070.
41 W. Yang, L. Luo, T. Chen and N. Wang, *Chem. Mater.*, 2005, **17**, 3883–3888.
42 L. O. P. Lsson and A. P. Monkman, *Adv. Mater.*, 2002, **14**, 757–758.